

Proton, Deuteron and (Resonant) Electron Polarimetry  
Richard Talman  
Laboratory for Elementary-Particle Physics  
Cornell University

22 January, 2018, Juelich

## 2 Outline

Proton-carbon, left-right scattering asymmetry polarimetry

Resonant electron polarimetry

- CEBAF polarized beam preparation

- Time domain beam structure and frequency domain spectra

Longitudinal polarization detection apparatus

- Local Lenz law (LLL) approximation

- Frequency choice

- Background rejection

Transverse, Stern-Gerlach polarimetry

- Calculated Stern-Gerlach (SG) deflection

- Beamline optics

Signal levels and noise suppression

### 3 Scattering asymmetry polarimetry

- ▶ High quality polarimetry will be critical to the success of any eventual measurement of the EDM of the proton (or any other particle.)
- ▶ But a thorough discussion of this topic deserves a dedicated paper and goes well beyond my expertise.
- ▶ All that is attempted in this section is to provide minimal information supporting motivations, choices, and arguments in other lectures.
- ▶ Especially deficient is the discussion of scattering asymmetry polarimetry, which is an area in which great progress toward the eventual EDM measurement goal has been made.

## 4 Scattering asymmetry polarimetry (continued)

- ▶ This section is included more to celebrate the success of a spin control experiment using carbon scattering asymmetry than to explain the polarimetry.
- ▶ References are given to papers describing the actual polarimetry.
- ▶ As a matter of fact, scattering asymmetry polarimetry is the only type of polarimetry that is currently known to have analysing power good enough to enable beam polarizations to be externally phase-locked and, therefore, stabilized.

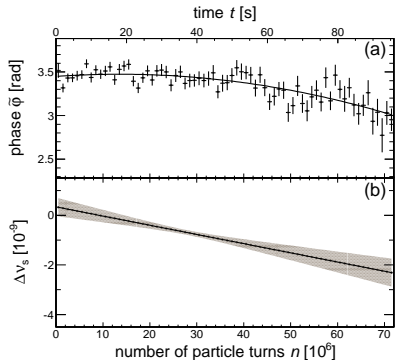


FIG. 3. (a): Phase  $\bar{\varphi}$  as a function of turn number  $n$  for all 72 turn intervals of a single measurement cycle for  $\nu_s^{\text{fix}} = -0.160975407$ , together with a parabolic fit. (b): Deviation  $\Delta\nu_s$  of the spin tune from  $\nu_s^{\text{fix}}$  as a function of turn number in the cycle. At  $t \approx 38$  s, the interpolated spin tune amounts to  $\nu_s = (-16097540771.7 \pm 9.7) \times 10^{-11}$ . The error band shows the statistical error obtained from the parabolic fit, shown in panel (a).

**Figure 1:** This figure, with its original figure number and caption, is copied from the Eversmann et al.[2] paper describing performed with a polarized 0.97 GeV deuteron beam at the COSY accelerator in Juelich, Germany.

- ▶ Since the scattering asymmetry analysing power is strongly dependent on particle energy, there is an element of chance concerning the availability of polarimetry for any particular particle at a particular energy.
- ▶ The asymmetry of 1 GeV kinetic energy deuteron scattering from carbon has excellent analysing power, which helped to make the Eversmann et al. measurement feasible.
- ▶ Unfortunately a polarized deuteron beam of this energy (or of any energy) cannot be frozen in a magnetic storage ring.
- ▶ As it happens, for proton-carbon scattering there is high, very nearly maximal, left-right asymmetry, for proton kinetic energies close to the proton frozen spin energy of 233 MeV in an electrostatic ring.

7

- ▶ The polarization of a 0.97 GeV deuteron beam was manipulated to lie in the horizontal plane at “phase angle”  $\tilde{\phi}$ , as measured by the deuteron-carbon scattering polarimeter. The MDM-induced precession causes  $\tilde{\phi}$  to advance rapidly.
- ▶ However, when viewed (stroboscopically) at a particular beam energy, there are beam energies at which the polarization appears (locally) to be “frozen” (like the spokes of a wagon wheel in a Western movie).
- ▶ This level of local frozen spin was good enough for the COSY beam control experiment to be performed.
- ▶ The importance of the COSY experiment can be inferred from the original figure caption (which has been copied along with the figure from the COSY paper)
- ▶ and from the final sentence of their abstract: “..., the spin tune was determined with a precision of the order of  $10^{-10}$  for a continuous 100 s accelerator cycle. This renders the presented method a new precision tool for accelerator physics: controlling the spin motion of particles to high precision, in particular for the measurement of electric dipole moments of charged particles in a storage ring”.
- ▶ The ability to measure spin tunes reproducibly with a fractional accuracy of, say,  $10^{-10}$ , implies the ability to measure an EDM torque that is weaker than the MDM torque by a factor as small as  $10^{-10}$ .

## 8 Phase-locked beam polarization control

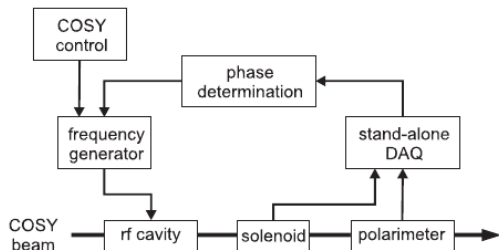


FIG. 2. Schematic layout of the feedback system. Based on the measured polarization direction in the polarimeter and the phase of the rf solenoid the control system adds an offset in the range of  $\pm 2$  Hz to the nominal value for the revolution frequency. The minimum step size is 3.7 mHz.

Figure 2: This figure, with its original figure number and caption, is copied from Hempelmann et al.[3].



## 9 Phase-locked beam polarization control (continued)

- ▶ Performance of the p-D polarimetry, and of the phase locking, is described in a recent publication of Hemplemann et al.[3].
- ▶ What makes this work truly remarkable, and probably unprecedented, is that a discrete scaler, registering the difference between left and right scatters, has been integrated into the electronic servomechanism controller shown by block diagram in Figure 2.
- ▶ The final sentence of this paper declares that “Such a capability meets a requirement for the use of storage rings to look for an intrinsic electric dipole moment of charged particles.”

## 10 Resonant electron polarimetry

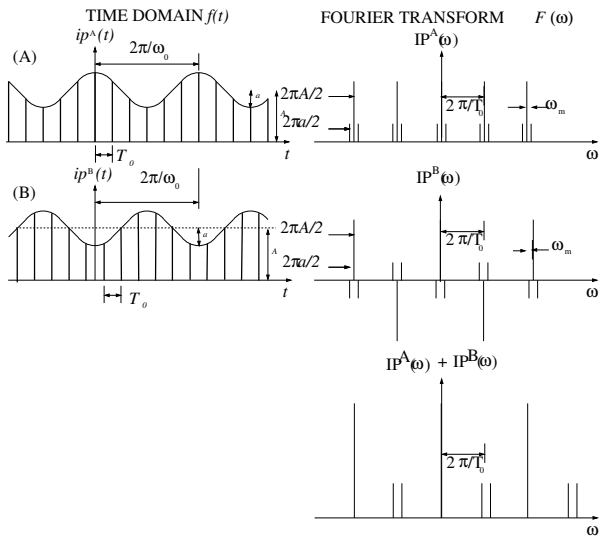
- ▶ Experiments are proposed at Jefferson Lab. to measure (first longitudinal, then, later, using Stern-Gerlach (SG) deflection, transverse) polarization of an electron beam by measuring the excitation induced in a resonant cavity,
- ▶ For both cases there are two major difficulties.
  - ▶ The Stern-Gerlach (SG) signals are very weak, making them hard to detect in absolute terms.
  - ▶ Even more serious is the smallness of the SG signals relative to imperfection-induced, direct excitation of the resonant detector
- ▶ In principle, with ideal resonator construction and positioning, the background would vanish. But, because the electron charge is so large relative to its magnetic moment, special beam preparation and polarization modulation are required to suppress this background.
- ▶ Beam preparation is described first.

## 11 CEBAF polarized beam preparation

- ▶ Dual CEBAF electron sources produce oppositely polarized A and B beams having bunch separation 4 ns. Interleaved, the resulting A & B beam has bunch separation 2 ns.
- ▶ The effect of this beam preparation is to produce a bunch charge repetition frequency of 0.5 GHz, different from the bunch polarization frequency of 0.25 GHz. With frequency domain spectral filtering this frequency separation will greatly enhance the foreground/background selectivity.
- ▶ Because linac bunches are short there is substantial resonator response at numerous strong low order harmonics of the 0.25 GHz bunch polarization frequency. The proposed SG responses are centered at odd harmonics,  
 $f_r = 0.25, 0.75, 1.25, \dots$  GHz.

- ▶ The absence of beam-induced detector response at these odd harmonics greatly improves the rejection of spurious “background” caused by bunch charge combined with apparatus imperfection and misalignment.
- ▶ For further background rejection the polarization amplitudes are modulated at a low, kHz, frequency, which shifts the SG response to sidebands of the central SG frequencies.
- ▶ Exactly the same beam preparation will be optimal both for resonant longitudinal polarimetry (described next) and transverse, SG-polarimetry, described later.
- ▶ Current and polarization time domain amplitudes are plotted on the left in the following figure; their frequency domain signals are plotted on the right.

# 13 Time domain beam structure and frequency domain spectra



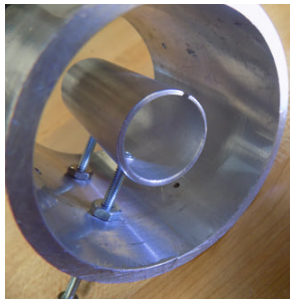
- ▶ The fundamental impediment to resonant electron polarimetry comes from the smallness of the ratio of magnetic moment divided by charge,

$$\frac{\mu_B/c}{e} = 1.930796 \times 10^{-13} \text{ m}; \quad (1)$$

except for a tiny anomalous magnetic moment correction and sign, the electron magnetic moment is equal to the Bohr magneton  $\mu_B$ .

- ▶ This ratio has the dimension of length because the Stern-Gerlach force due to magnetic field acting on  $\mu_B$ , is proportional to the *gradient* of the magnetic field.
- ▶ To the extent that it is “natural” for the magnitudes of  $E$  and  $cB$  to be comparable, Stern-Gerlach forces are weaker than electromagnetic forces by ratio (1). This adverse ratio needs to be overcome (by beam, apparatus, and field preparation and alignment), in order for MDM excitation to exceed direct charge excitation “background”.

## 15 Longitudinal polarization



- ▶ A basic resonator cell is a several centimeter long copper split-cylinder, with gap serving as the capacitance  $C$  of, for example, a 1.75 GHz  $LC$  oscillator, with inductance  $L$  provided by the conducting cylinder acting as a single turn solenoid.
- ▶ The photos show split-ring resonators (open at the ends for visibility) built and tested at UNM, resonant at 2.5 GHz, close to the design frequency.
- ▶ The resonator design (by Hardy and Whitehead in 1981) and has been widely used for NMR measurements.

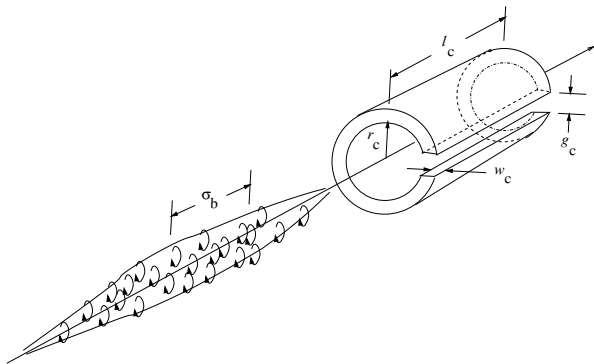


**Figure 3:** Perspective view of polarized beam bunch passing through the polarimeter. Dimensions are shown for the polarized proton bunch and the split-cylinder copper resonator. For the proposed test, using a polarized electron beam at Jefferson Lab, the bunch will actually be substantially shorter than the cylinder length, and have a beer can shape.



- ▶ A frequency  $f_0$  train of longitudinally polarized bunches of electrons in a linac beam passes through the split-cylinder resonator.
- ▶ The split cylinder can be regarded as a one turn solenoid.
- ▶ The bunch polarization toggles, bunch-to-bunch, between directly forward and directly backward.
- ▶ The resonator harmonic number relative to  $f_0$  is an odd number in the range from 1 to 11. (Actually 11 has been adopted.)
- ▶ This beam preparation immunizes the resonator from direct charge excitation. Irrespective of polarization, the A+B-combined bunch-charge frequencies will consist only of harmonics of  $2f_0 = 0.5$  GHz, incapable of exciting the resonator(s).

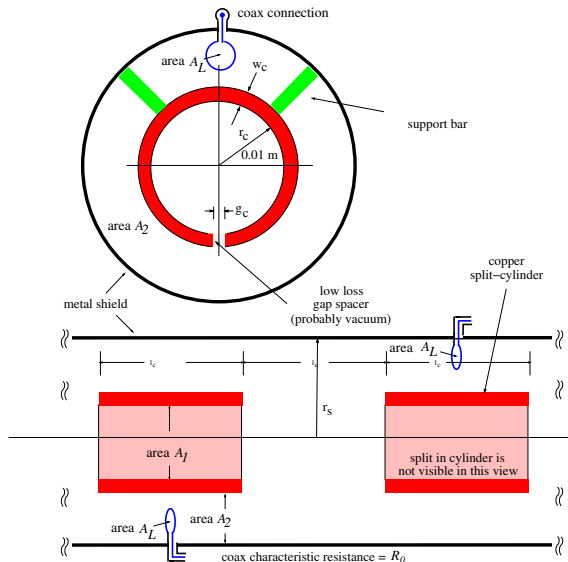
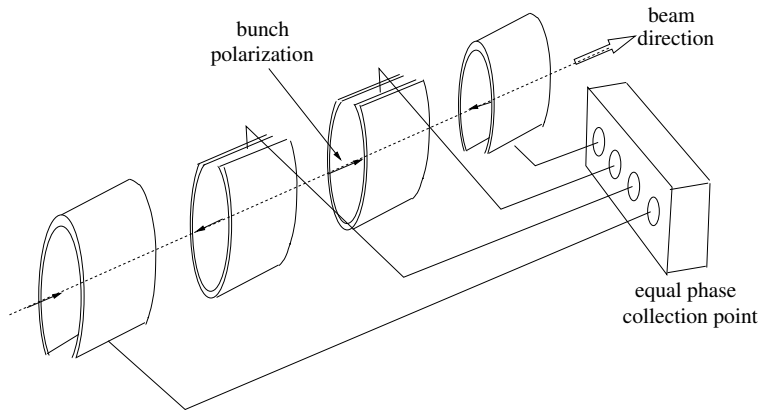
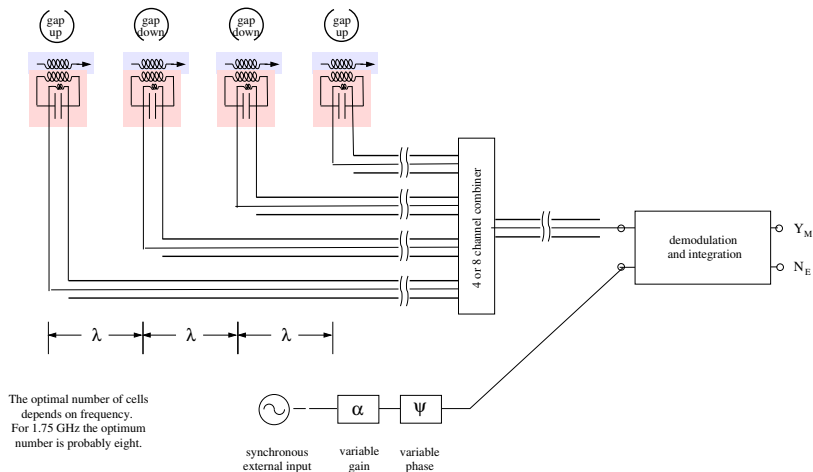


Figure 4: End and side views of two resonant split-cylinder polarimeter cells. Signals from individual resonators are loop-coupled out to coaxial cables and, after matched delay, added.



**Figure 5:** Sketch showing beam bunches passing through multiple resonators. Cable lengths are arranged so that beam polarization signals add constructively, but charge-induced, asymmetric-resonator excitations cancel.



**Figure 6:** Circuit diagram for a circuit that coherently sums the signal amplitudes from four (or eight) polarimeter cells. Excitation by passing beam bunches is represented by inductive coupling. Quadrature signal separation routes in-phase signals to the  $Y_E$  ("Yes it is magnetic-induced") output, and out-of-phase, quadrature signals to the  $N_E$  ("No it is electric-induced") output. The external coherent signal processing functionality to achieve this separation is indicated schematically by the box labelled "demodulation and integration". Unfortunately the performance is not as clean as the terminal names imply.

- ▶ Four such cells, regularly arrayed along the beam, form a half-meter-long polarimeter.
- ▶ The magnetization of longitudinally-polarized electron bunches passing through the resonators coherently excites their fundamental oscillation mode and the coherently-summed “foreground” response from all resonators measures the polarization.
- ▶ “Background” due to direct charge excitation has been suppressed by arranging successive beam bunches to have alternating polarizations. This has moved the beam polarization frequency away from the direct beam charge frequency.
- ▶ Charge-insensitive resonator design, modulation-induced sideband excitation, and synchronous detection, permit the magnetization foreground to be isolated from spurious, charge-induced background.

## 22 Constructive superposition of resonant excitations

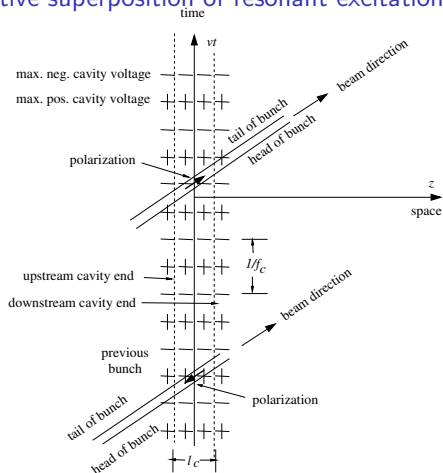


**Figure 7:** Space-time plot showing entry by the front, followed by exit from the back of one bunch, followed by the entrance and exit of the following bunch. Bunch separations and cavity length are arranged so that cavity excitations from all four beam magnetization excitations are perfectly constructive. The rows ++++ and ---- represent equal time contours of maximum or minimum  $V_C$ ,  $E_\phi$ ,  $dB_z/dt$ , or  $dl_C/dt$ , all of which are in phase..

## 23 Resonator parameters

- ▶ Treated as an  $LC$  circuit, the split cylinder inductance is  $L_c$  and the gap capacity is  $C_c$ . The highly conductive split-cylinder can be treated as a one-turn solenoid.
- ▶ For simplicity, minor corrections due to the return flux are not included in formulas given shown here
- ▶ In terms of its current  $I$ , the magnetic field  $B$  is given by

$$B = \mu_0 \frac{I}{l_c}, \quad (2)$$

- ▶ The magnetic energy  $W_m$  can be expressed in terms of  $B$  or  $I$ ;

$$W_m = \frac{1}{2} \frac{B^2}{\mu_0} \pi r_c^2 l_c = \frac{1}{2} L_c I^2. \quad (3)$$

- 24 ▶ The self-inductance is therefore

$$L_c = \mu_0 \frac{\pi r_c^2}{l_c}. \quad (4)$$

- ▶ The gap capacitance (with gap  $g_c$  reckoned for vacuum dielectric and fringing neglected) is

$$C_c = \epsilon_0 \frac{w_c l_c}{g_c}. \quad (5)$$

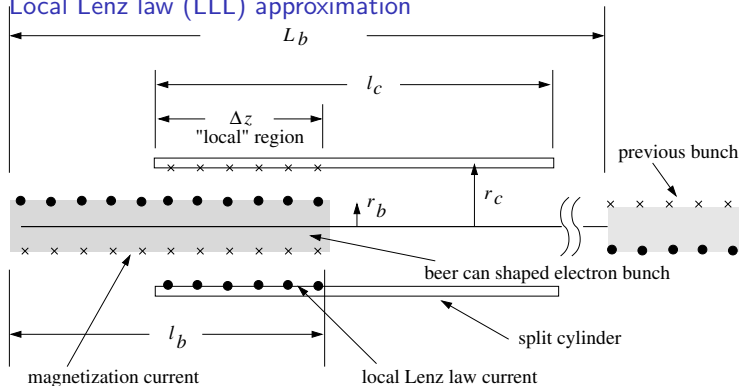
- ▶ Because the numerical value of  $C_c$  will be small, this formula is especially unreliable as regards its separate dependence on  $w_c$  and  $g_c$ .
- ▶ Furthermore, for low frequencies the gap would contain dielectric other than vacuum.
- ▶ Other resonator parameters, with proposed values, are given in following tables.



parameter name	parameter symbol	formula	unit	value
cylinder length	$l_c$		m	0.04733
cylinder radius	$r_c$		m	0.01
gap height	$g_c$		m	0.00103943
wall thickness	$w_c$		m	0.002
capacitance	$C_c$	$\epsilon_0 \frac{w_c l_c}{g_c \epsilon_r}$	pF	0.47896
inductance	$L_c$	$\mu_0 \frac{\pi r_c^2}{l_c}$	nH	7.021 3
resonant freq.	$f_c$	$1/(2\pi\sqrt{L_c C_c})$	GHz	2.7445
resonator wavelength	$\lambda_c$	$c/f_c$	m	0.10923
copper resistivity	$\rho_{Cu}$		ohm-m	1.68e-8
skin depth	$\delta_s$	$\sqrt{\rho_{Cu}/(\pi f_c \mu_0)}$	$\mu\text{m}$	1.2452
eff. resist.	$R_c$	$2\pi r_c \rho_{Cu}/(\delta_s l_c)$	ohm	0.017911
unloaded. qual. factor	$Q$			6760.0
effective qual. fact.	$Q/h_c$			643.65
bunch frequency	$f_A = f_B = f_0$		GHz	0.2495
cavity harm. number	$h_c$	$f_c/f_0$		11
electron velocity	$v_e$	$c\sqrt{1 - (1/2)^2}$	m/s	2.5963e8
cavity transit time	$\Delta t$	$l_c/v_e$	ns	0.18230
transit cycle advance	$\Delta\phi_c$	$f_c \Delta t$		0.50032
entry cycle advance		$\Delta\phi_c l_b/l_c$		0.15011
electrons per bunch	$N_e$			$2.0013 \times 10^6$
bunch length	$l_b$		m	0.0142
bunch radius	$r_b$		m	0.002

**Table 1:** Resonator and beam parameters. The capacity has been calculated using the parallel plate formula. The true capacity is somewhat greater, and the gap  $g_c$  will have to be adjusted to tune the natural frequency. When the A and B beam bunches are symmetrically interleaved, the bunch repetition frequency (with polarization ignored) is  $2f_0$ .

## 26 Local Lenz law (LLL) approximation



- ▶ A local Lenz law approximation for calculating the current induced in split cylinder by an electron bunch entering a split-cylinder resonator, treated as a one turn solenoid
- ▶ The electron bunch is assumed to have a beer can shape, with length  $l_b$  and radius  $r_b$ .
- ▶ Lenz's law is applied to the local overlap region of length  $\Delta z$ .
- ▶ Flux due to the induced Lenz law current exactly cancels the flux due to the Ampère bunch polarization current.

- ▶ The magnetization  $\mathbf{M}$  within length  $\Delta z$  of a beam bunch (due to all electron spins in the bunch pointing, say, forward) is ascribed to azimuthal Ampèrian current  $\Delta I_b = i_b \Delta z$ .
- ▶ The bunch transit time is shorter than the oscillation period of the split cylinder and the presence of the gap in the cylinder produces little suppression of the Lenz's law current
- ▶  $\Delta I_{LL} = i_{LL} \Delta z$  is the induced azimuthal current shown in the (inner skin depth) of the cylinder
- ▶ To prevent any net flux from being present locally within the section of length  $\Delta z$ , the flux due to the induced Lenz law current must cancel the Ampère flux.

- ▶ Lenz law current per longitudinal length  $i_{LL}$  induces Lenz law magnetic field  $B_{LL} = \mu_0 i_{LL}$  causing magnet flux through the cylinder

$$\phi_{LL} = \mu_0 \pi r_c^2 i_{LL}. \quad (6)$$

- ▶ Jackson says the magnetic field  $\mathbf{B}_b$  within the polarized beam bunch is equal to  $\mu_0 \mathbf{M}_b$  which is the magnetization (magnetic moment per unit volume) due to the polarized electrons.

$$B_b = \mu_0 M_B = \mu_0 \frac{N_e \mu_B}{\pi r_b^2 l_b}, \quad (7)$$

where  $N_e$  is the total number of electrons in each bunch.

- ▶ The flux through ring thickness  $\Delta z$  of this segment of the beam bunch is therefore

$$\phi_b = B_b \pi r_b^2 = \mu_0 \frac{N_e \mu_B}{l_b}, \quad (8)$$

- ▶ Since the Lenz law and bunch fluxes have to cancel we obtain

$$i_{LL} = -\frac{N_e \mu_B}{l_b} \frac{1}{\pi r_c^2}. \quad (9)$$

- ▶ For a bunch that is longitudinally uniform (as we are assuming) we can simply take  $\Delta z$  equal to bunch length  $l_b$  to obtain

$$I_{LL} = i_{LL} l_b = -\frac{N_e \mu_B}{\pi r_c^2} \quad (10)$$

- ▶ With bunch fully within the cylinder,  $I_{LL}$  “saturates” at this value.

- ▶ The bunch is short (i.e.  $l_b \ll l_c$ ) so the linear build up of  $I_{LL}$  can be ascribed to a constant applied voltage  $V_{LL}$  required to satisfy Faraday's law.
- ▶ For a CEBAF  $I_e = 160 \mu\text{A}$ , 0.5 GHz bunch frequency beam the number of electrons per bunch is approximately  $2 \times 10^6$  and the Lenz law current is

$$I_{LL}^{\max} = -\frac{N_e \mu_B}{\pi r_c^2} \left( \stackrel{\text{e.g.}}{=} -5.9078 \times 10^{-14} \text{ A} \right). \quad (11)$$

- ▶ The same excess charge is induced on the capacitor during the bunch exit from the cylinder at which time the resonator phase has reversed.
- ▶ The total excess charge that has flowed onto the capacitor due to the bunch passage is

$$Q_1^{\max.} \approx I_{LL}^{\text{sat.}} \frac{l_b}{v_e} \left( \stackrel{\text{e.g.}}{=} -3.2312 \times 10^{-24} \text{ C} \right). \quad (12)$$

31

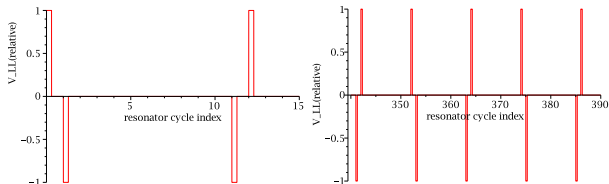
- ▶ If there were no further resonator excitations, the charge on the capacitor would oscillate between  $-Q_1^{\max.}$  and  $+Q_1^{\max.}$ .
- ▶  $U_1^{\text{pol.}}$ , the corresponding resonator energy, is the “foreground” quantity that (magnified by a resonant amplitude build-up factor  $M_r^2$ ) provides the polarization measure in the form of steady-state energy  $U^{\text{pol.}}$  stored on the capacitor;

$$U^{\text{pol.}} = \frac{1}{2} \frac{Q_1^{\max.2}}{C_c} M_r^2 = \left( M_r^2 \times 1.0899 \times 10^{-35} \text{ J} \right) \quad (13)$$

$Q_1^{\max.} = 3.2312 \times 10^{-24} \text{ C}$  is the charge deposited on the resonator capacitance during a single bunch passage of a bunch with the nominal ( $N_e = 2 \times 10^6$  electrons) charge.

## 32 Lumped circuit analysis of resonant build-up

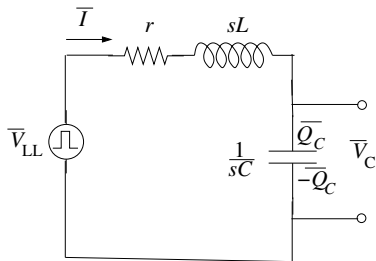
- ▶ In a MAPLE program the excitation is modeled using “piecewise defined” trains of pulses. Bipolar pulses modeling entry to and exit from the resonator are obtained as the difference between two, time-displaced “top hat” pulse trains



- ▶ Pulsed excitation voltage pulse are caused by successive polarized bunch passages through the resonator.
- ▶ A few initial pulses are shown on the left, some later pulses are shown on the right.
- ▶ The units of the horizontal time scale are such that, during one unit along the horizontal time axis, the natural resonator oscillation phase advances by  $\pi$ . The second pulse starts exactly at 1 in these units
- ▶  $h_c=11$  units of horizontal scale advance corresponds to a phase advance of  $\pi$  at the  $f_A = f_B = f_0 = 0.2495$  GHz “same-polarization repetition frequency” .



- ▶ Lumped constant representation of the split-cylinder resonator as a parallel resonant circuit is shown



- ▶ Voltage division in this series resonant circuit produces capacitor voltage transform  $\bar{V}_C(s)$ ;

$$\bar{V}_C(s) = \frac{1/(Cs)}{1/(Cs) + r + Ls} \bar{V}_{LL}(s) = \frac{\bar{V}_{LL}(s)}{1 + rs + CLs^2}. \quad (14)$$

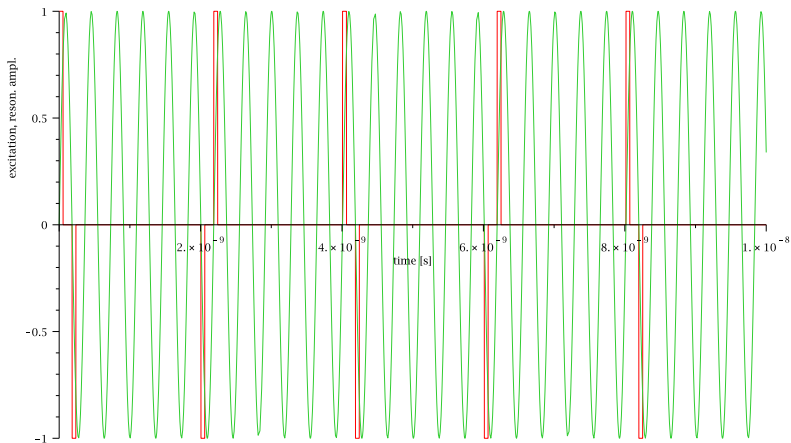


**Figure 8:** Alternating polarization excitation pulses superimposed on resonator response amplitude and plotted against time. Bunch separations are 2 ns, bunch separation between same polarization pulses is 4 ns. The vertical scale can represent  $V_C$ ,  $E_\phi$ ,  $dB_z/dt$ , or  $dI_C/dt$ , all of which are in phase.

This comparison shows that the response is very nearly in phase with the excitation.

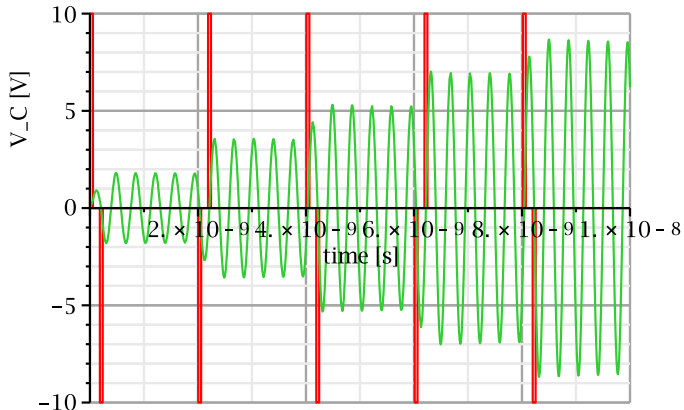


**Figure 9:** Accumulating capacitor voltage response  $V_C$  while the first five linac bunches pass the resonator. The accumulation factor relative to a single passage, is plotted.

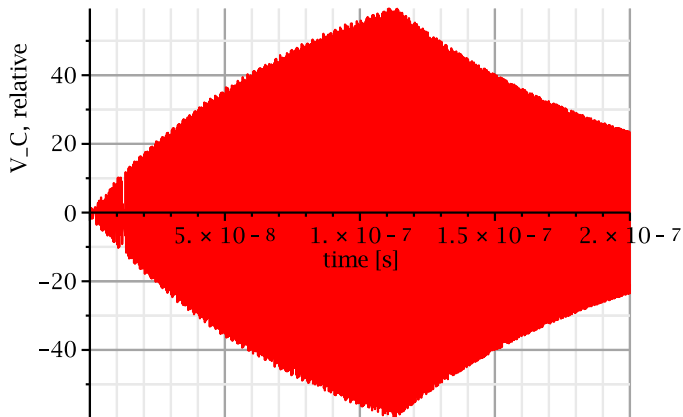


**Figure 10:** Relative resonator response to a train of beam pulse that terminates after about 110 ns. After this time the resonator rings down at roughly the same rate as the build-up. The circuit parameters are those given in Table 1, except that the resistance for the plot is  $r = 10r_c$ . The true response build up would be greater by a factor of 10, over a 10 times longer build-up time.

## 37 Frequency choice

parameter	symbol	unit	3	5	7	9	11
harmonic numb.	$h_c$	GHz	3	5	7	9	11
A,B bunch freq.	$f_0$	GHz	0.2495	0.2495	0.2495	0.2495	0.2495
resonant freq.	$f_0$	GHz	0.7485	1.2475	1.7465	2.2455	2.7445
dielectric			polyeth.	polyeth.	vacuum	vacuum	vacuum
rel. diel. const.	$\epsilon_r$		2.30	2.30	1.00	1.00	1.00
numb. cells/m	$N_{cell}$	$\approx$ /m	4	4	4	4	4
band width	$f_c/Q$	kHz	286	277	309	351	388
quality factor	$Q$		2.61e+03	4.51e+03	5.65e+03	6.40e+03	7.08e+03
effective qual. fact.	$M_r = Q/h_c$		8.72e+02	9.01e+02	8.07e+02	7.12e+02	6.44e+02
cyl. length	$l_c$	cm	17.35	10.41	7.44	5.78	4.733
cyl. radius	$r_c$	cm	1.0	1.0	1.0	1.0	1.000
gap height	$g_c$	mm	1.305	2.021	0.709	1.171	1.750
wall thickness	$w_c$	mm	10.0	5.0	2.0	2.0	2.0
capacitance	$C_c$	pF	27.076	5.245	1.859	0.874	0.479
inductance	$L_c$	nF	1670	3.10	4.47	5.74	7.02
skin depth	$\delta_s$	$\mu m$	2.384	1.847	1.561	1.377	1.245
effective resistance	$R_c$	m $\Omega$	2.55	5.49	9.09	13.26	17.91
cav. trans. time	$\Delta_t$	ns	0.668	0.401	0.286	0.223	0.182
entry cycle adv.	$\Delta_t f_c l_b / l_c$		0.041	0.068	0.096	0.123	0.150
single pass energy	$U_{1,max}$	J	1.9e-37	1.0e-36	2.8e-36	6.0e-36	1.1e-35
sat. cap. volt.	$V_{C,sat}$	V	1.0e-10	5.6e-10	1.4e-09	2.6e-09	4.3e-09
sat. cap. charge	$Q_{C,sat}$	C	2.8e-21	2.9e-21	2.6e-21	2.3e-21	2.1e-21
sat. ind. curr.	$I_{L,sat}$	A	1.3e-11	2.3e-11	2.9e-11	3.2e-11	3.6e-11
signal power	$P_{sig}$	W	4.39e-22	4.03e-21	1.28e-20	2.72e-20	5.0e-20
therm. noise floor @1s	$P_{noise}$	W	4.05e-21	4.05e-21	4.05e-21	4.05e-21	4.05e-21
signal/noise at 1 s	$\log_{10}(P_{sig}/P_{noise})$	db	-9.65	-0.01	4.99	8.27	10.88
signal/noise at 100 s	" + 20	db	10.35	19.99	24.99	28.27	30.88

## 38 Background rejection

misalignment	misalignment factor formula	installation specification	operational improvement factor	background reduction factor
beam position	$\sqrt{\sigma_x^2 + \sigma_y^2}$	< 0.001 m	/10 <sup>2</sup>	1e-5
beam slope	$\sqrt{\sigma_{x'}^2 + \sigma_{y'}^2}$	< 0.001	/10	1e-4
A/B imbalance	$\Delta I_{ave}/I_{ave}$	< 0.01	/10	1e-3
pol. modulate	$S^{pol.}$		/10	1e-1
slope modul	$S^{m.a.}$		/10	1e-1
noise/signal	$10^{10} S^{m.a.} S^{pol.} W_1^{m.a.}/U^{pol.}$			1e-4

- ▶ The expected saturation level resonator voltage is

$$V_C^{rcvr.} = \frac{N_{cell}(Q/h_c) Q_1^{sat.}}{C_c} = 4.34 \times 10^{-9} \text{ V.} \quad (15)$$

- ▶ Accumulated over 100s, this is expected to be 31 db above the thermal noise floor in a room temperature copper cavity.

### 39 Transverse, Stern-Gerlach polarimetry

A Jefferson Lab test is also proposed to detect Stern-Gerlach (SG) electron deflection in a polarimeter consisting of 8 small bore permanent magnet quadrupoles like this.

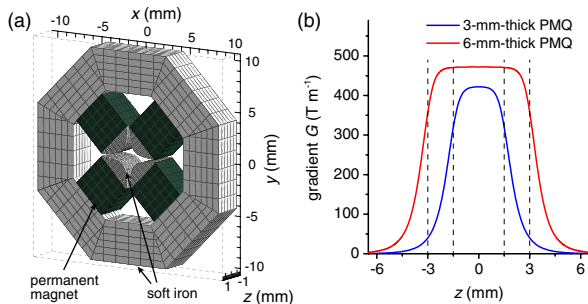
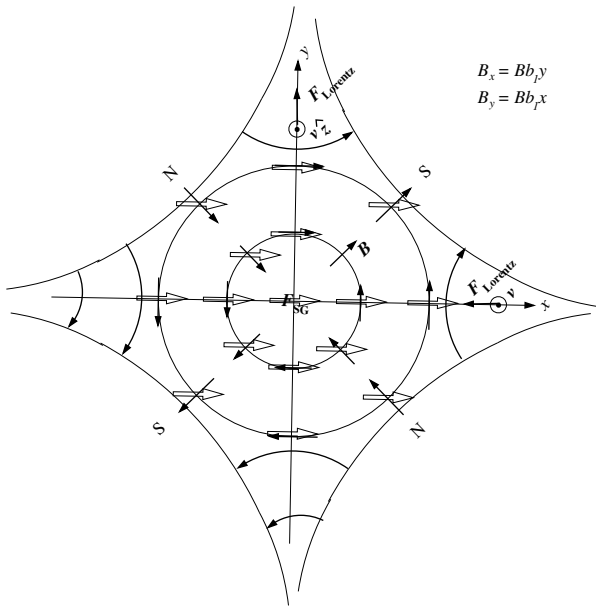


FIG. 5. (a) RADIA model of a 3-mm-thick PMQ magnet and (b) the calculated on-axis focusing gradient of a 3-mm and a 6-mm PMQ. Dashed lines indicate the physical boundaries of the 3- and 6-mm-thick PMQs.

## 40 Stern-Gerlach orbit deflection in a quadrupole



$$\uparrow \quad s \circ \mathbf{B} = Bb_1x$$

$$s = \hat{y}$$

$$F_{\text{SG}} = \mu \nabla (s \circ \mathbf{B})$$

$$= \mu \hat{x} \frac{\partial}{\partial x} Bb_1x$$

$$= \mu Bb_1 \hat{x}$$

$$\longrightarrow \quad s \circ \mathbf{B} = Bb_1y$$

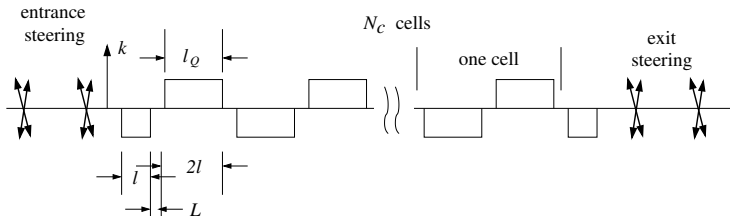
$$s = \hat{x}$$

$$F_{\text{SG}} = \mu \nabla (s \circ \mathbf{B})$$

$$= \mu \hat{y} \frac{\partial}{\partial y} Bb_1y$$

$$= \mu Bb_1 \hat{y}$$





- ▶ Parameter values for numerical calculations in this talk:
  - quadrupole length  $l_Q = 2l = 0.02$  m
  - quadrupole separation  $L = 0.005$  m
  - number of FODO cells  $N_c = 4$
- ▶ Entrance and exit steering is needed to correct for quadrupole misalignment steering.
- ▶ Positive detection would “refute” the Bohr-Pauli assertion that the Stern-Gerlach experiment cannot be performed with electrons.

- ▶ But not really!
- ▶ The quotation marks on “refute” acknowledge that Bohr and Pauli had no knowledge of modern technical capabilities
- ▶ More important, the most essential aspect of their claim—that electrons cannot be “separated” by their spin state with an SG apparatus—is not disputed—polarization-independent defocusing of the (finite-emittance) beam dwarfs any achievable separation into a spin-up and a spin-down beam
- ▶ It should, however, be possible to measure the polarization state of an electron beam by measuring its bunch-magnetization centroid deflection
- ▶ This is what needs to be demonstrated
- ▶ If and when it is demonstrated, a high analysing power, non-destructive form of (transverse) polarimetry will have been demonstrated

- ▶ For the initial test described in this talk I choose  $N_c = 4$  but, for an eventual apparatus,  $N_c$  could be several times greater, depending on tolerance issues to be discussed.
- ▶ Since the design uses permanent magnets, any realization of the design is static, specific to a particular electron beam energy.
- ▶ But the design scales easily to other energies and parameter choices.
- ▶ The assumed quadrupoles are patterned after permanent magnet quadrupoles described in papers by Li, Musumeci, Maxson and others

#### 44 Calculated SG deflection

- ▶ During passage through a short quadrupole, the bend radius is determined by the centripetal force equation,

$$\frac{pv}{r} = evB = ev \frac{\partial B_x}{\partial x} x$$

- ▶ Re-arranging this equation, the integrated particle deflection angle during passage is

$$\theta = \frac{l_Q}{r} = \frac{cl_Q \langle \partial B_x / \partial x \rangle x}{pc/e},$$

- ▶ For a quadrupole of strength (i.e. inverse focal length)  $q = 1/f$ , the deflection angle is  $\pm qx$  where

$$q = \pm \frac{\theta}{x} = \pm C_\gamma (3 \times 10^8) / (0.511 \times 10^6) \left[ \frac{l_Q \langle \partial B_x / \partial x \rangle}{\gamma_e} \right]$$
$$\approx \pm 587 \text{T}^{-1} \text{m}^{-1} \left[ \frac{l_Q \langle \partial B_x / \partial x \rangle}{\gamma_e} \right].$$

- ▶ The  $\gamma_e$  factor inside the square bracket “cancels” the momentum dependence, allowing the lens strength to be expressed as an inverse focal length.
- ▶ (For fully relativistic electrons) the lens can be treated as purely geometric (i.e. independent of momentum) by varying  $\partial B_x/\partial x$  proportional to  $\gamma_e$ ,
- ▶ but only until the gradient cannot be increased further !
- ▶ For this talk I take  $l_q = 0.02$  m and (already achievable) field gradient  $\partial B_x/\partial x = 500$  T/m as nominal values.
- ▶ Higher field gradient,  $\partial B_x/\partial x = 1000$  T/m, at shorter length,  $l_Q = 0.01$  m is expected to be achievable.
- ▶ This would yield the same length-strength product of 10 T, but be more useful in the (important) sense of allowing a lens of the same strength to be shorter relative to its focal length.

- ▶ Limited only by the maximum achievable permanent magnetic field gradient, even with careful element alignment and coherent multiplication of the displacement by the number of quadrupoles in the beamline, the Stern-Gerlach deflection can be expected to be only comparable in magnitude with deflection caused by misaligned quadrupoles.
- ▶ This spurious excitation will be suppressed by the interleaving of opposite-polarization A and B beams.
- ▶ This shifts the spectral frequency of the SG deflection to one half the spectral frequency of the spurious deflection,
- ▶ This will allow the SG contribution to be isolated in a frequency-sensitive BPM.

## 47 Beamline optics

Optical properties of the proposed beamline are shown in the following figures.

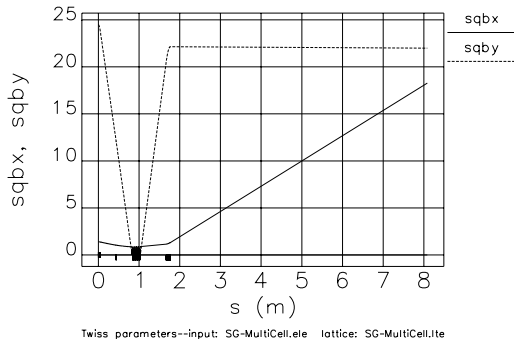


**Figure 11:** Beta functions for the Stern-Gerlach detection beamline. The length of the beamline is as long as possible consistent with the requirement that the rms beam size is conservatively smaller than the vacuum chamber radius. An SG-detecting BPM is located as far along the beam line as possible.

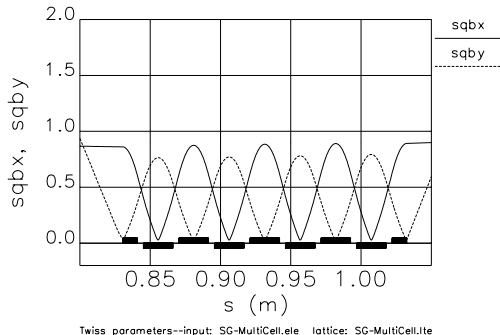


**Figure 12:** Optics in the periodic, SG deflection, multiple cell FODO lattice. The full quadrupole lengths are  $l_Q = 2l = 0.02$  m and the quad separation distances are  $L = 0.005$  m. So the full cell length is  $L_{\text{cell}} = 0.05$  m.

- ▶ Only  $N_c = 4$  cells for the FODO section are shown.
- ▶ but  $N_c$  could be increased with little effect on the matching.
- ▶  $N_c$  is limited, however, by the fact that the same optics that magnifies the SG deflection also magnifies the sensitivity to transverse beam displacement injection error.



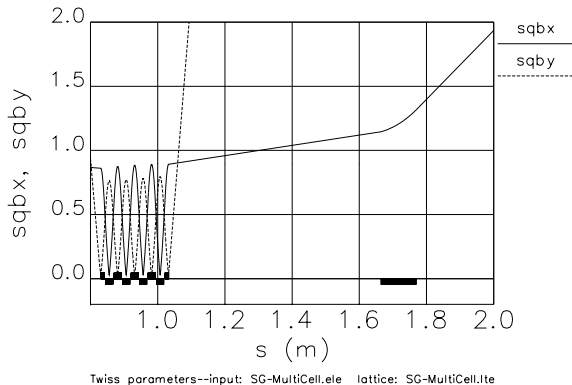


**Figure 13:** The quadrupole at  $s = 1.72$  m (at a distance  $L_{\text{coll.}} = 0.8$  m from the center of the FODO lattice) is needed to restrict the growth of the defocussed transverse coordinate. But it also has the beneficial effect of magnifying the SG deflection. At low electron energy the beam emittance may limit the exit drift length to be shorter than shown to prevent beam loss before the beam passes through the BPM's.

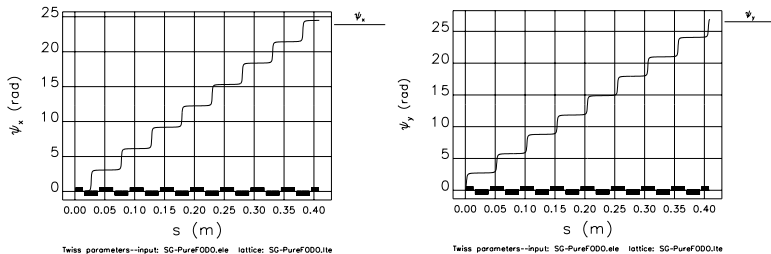


**Figure 14:** Phase advances  $\psi_x$  and  $\psi_y$  through a lattice with  $N_c = 8$  cells. Since  $25/8 = 3.125$ , one sees that the phase advances per half cell are quite close to the value of 180 degrees, the maximum value that could be stable for arbitrarily large value of  $N_c$ . It is also the value for which all SG deflections superimpose constructively.

## 51 Dependence on electron energy

- ▶ Adiabatic damping causes the beam emittances to shrink proportional to  $\gamma_e$
- ▶ For fixed  $q$ , this produces a  $\gamma_e^{1/2}$  SG enhancement factor with increasing  $\gamma_e$ .
- ▶ This capability “saturates” when the quadrupole strength required to produce the necessary focal length is no longer physically achievable.

- ▶ Using the ELEGANT program, the focal lengths of the individual quadrupoles in the FODO line tuned for  $\pi$  phase advance per half cell are

$$q = kl_Q = 68.1 \text{ m}^{-1}.$$

- ▶ The corresponding focal length is  $f = 0.0147 \text{ m}$  —about 0.3 times the full cell length, as seems about right.
- ▶ Substitution of this  $q$  value and  $l_Q = 0.02$  and rearranging produces

$$l_Q \langle \partial B_x / \partial x \rangle = \frac{68.1 \text{ m}^{-1}}{587 \text{ T}^{-1} \text{ m}^{-1}} \gamma_e, \quad \text{or} \quad \left\langle \frac{\partial B_x}{\partial x} \right\rangle = \frac{68.1 \text{ m}^{-1}}{0.02 \text{ m} \times 587 \text{ T}^{-1} \text{ m}^{-1}}$$

If the practical limit for  $\partial B_x / \partial x$  is  $500 \text{ T/m}$ , then the apparatus being described could act as a Stern-Gerlach polarimeter up to  $\gamma_e = 86$ , or electron energy of  $43 \text{ MeV}$ .

### 53 Stern-Gerlach displacement

- ▶ The Stern-Gerlach deflection in a quadrupole is strictly proportional to the inverse focal lengths of the quadrupole;

$$\Delta\theta_x^{SG} = \frac{\mu_x^*}{ec\beta} q_x, \quad \text{and} \quad \Delta\theta_y^{SG} = \frac{\mu_y^*}{ec\beta} q_y.$$

- ▶ The magnetic moments  $\mu_x^*$  and  $\mu_y^*$  differ from the Bohr magneton  $\mu_B$  only by  $\sin\theta$  and  $\cos\theta$  factors respectively
- ▶ For a single quadrupole, the Stern-Gerlach-induced angular deflection is

$$\Delta\theta^{SG} = (1.93 \times 10^{-13} \text{ m}) q.$$

To determine the downstream displacement, one can use linear transfer matrix evolution;

$$\begin{pmatrix} \Delta x_{SG} \\ \cdot \end{pmatrix} = \begin{pmatrix} 1 & L_{\text{drift}} \\ 0 & 1 \end{pmatrix} \begin{pmatrix} 1 & 0 \\ 1.49 & 1 \end{pmatrix} \begin{pmatrix} 1 & L_{\text{coll}} \\ 0 & 1 \end{pmatrix} \begin{pmatrix} 0 \\ \Delta\theta_{SG} \end{pmatrix},$$

- ▶ The collimating quadrupole strength is 1.49 /m. Completing the matrix multiplication yields

$$\Delta x_{SG} = (0.8 + 2.19L_{\text{drift}})\Delta\theta_{SG}.$$

- ▶ The horizontal SG displacement is then given by

$$\begin{aligned}\Delta x_{SG} &= \pm 2N_c (1.93 \times 10^{-13} \text{ m}) \times 68.1 \text{ m}^{-1} (0.8 \text{ m} + 2.19L_{\text{drift}}) \\ &= 1.59 \times 10^{-9} \text{ m}.\end{aligned}$$

- ▶ The  $\pm$  factor doubles the SG displacement to 3.2 nm; because the BPM is tuned to half the bunch passage frequency, it responds constructively to the oppositely polarized A and B beam bunches.

## 55 Energy dependence of transverse polarimetry





- ▶ Expressing the quadrupole strength as an inverse focal length, as we have done, has had the effect of making the SG deflection independent of  $\gamma$ .
- ▶ Transverse beam size adiabatic damping enhances the energy dependence by a factor  $\sqrt{\gamma}$ .
- ▶ Even with the magnetic field gradient limited, the SG quadrupole lengths can be increased to preserve the optics described in this note, though with a longer FODO section.
- ▶ So the actual scaling with energy is such that the maximum achievable Stern-Gerlach deflection increases as  $\sqrt{\gamma}$  until the gradient can no longer be increased, and falls as  $1/\sqrt{\gamma}$  as the electron energy is increased from there.
- ▶ As for the test at CEBAF, the most convenient energy remains to be determined. Discussions so far have assumed 500 KeV electron kinetic energy, but this is for reasons of economy and accessibility, not because the SG signal is strongest at low energy. For the geometric parameters assumed in this note, the magnetic field gradient for  $\gamma_e = 2$  would be 12 T/m, far less than the maximum possible.








## 56 Signal levels and noise suppression





- ▶ The resonant BPM relies on precise, on-axis, alignment of a cavity tuned to have an anti-symmetric mode at the bunch charge passage frequency.
- ▶ Extreme selectivity is needed to separate the beam polarization signal from the spurious direct beam charge signal (and misaligned equipment).
- ▶ Also the signal power induced in the position-sensitive cavity by SG-induced displacement has to exceed the inherent thermal noise “floor”. This noise floor could, if necessary, be lowered by using liquid Helium temperature apparatus, but our estimates indicate that such an extreme measure is unnecessary.



- ▶ Pusch et al. report BPM measurement at the 0.1 mm level for beam currents greater than 250 pA. The J-Lab current is a million times greater. The off-axis shunt impedance of a resonant cavity is proportional to the square of the (beam-current  $\times$  beam-displacement) product. By this estimate, the resonator excitation of 1 Å will be at the noise floor. The SG displacement predicted for our beamline is approximately 30 Å.
- ▶ International Linear Collider motivated BPM performance design studies have shown that the  $\pm 20$  Å beam position pulse-to-pulse reproducibility planned for effective ILC operation will be achievable.
- ▶ A CEBAF beam is CW, with average current about five orders of magnitude higher than for the BPM test at the KEK, ATF Test Facility. Averaging over longer times can reduce some noise sources. For these, the increased average beam current can improve the signal to noise by the square root of the current ratio.
- ▶ Also the ILC cavity discharging time is far shorter than the ATF repetition period, which makes it necessary for them to treat their BPM resonant response on a pulse-by-pulse basis.
- ▶ Our high bunch frequency permits phase-sensitive CW signal treatment.

-  R. Talman, *The Electric Dipole Moment Challenge*, IOP Publishing, 2017
-  D. Eversmann et al., *New method for a continuous determination of the spin tune in storage rings and implications for precision experiments*, Phys. Rev. Lett. **115** 094801, 2015
-  N. Hempelmann et al., *Phase-locking the spin precession in a storage ring*, P.R.L. **119**, 119401, 2017
-  W. Hardy and L. Whitehead, *Split-ring resonator for use in magnetic resonance from 200-2000 MHz*, Review of Scientific Instruments, **52** (2) 213, 1981
-  B. R. Johnson, *Nuclear Spin Waves in Spin-Polarized Hydrogen*, Cornell Ph.D. thesis, 1984
-  Storage Ring EDM Collaboration, *A Proposal to Measure the Proton Electric Dipole Moment with  $10^{-29}$  e-cm Sensitivity*, October, 2011

-  J. Jackson, *Classical Electrodynamics*, 3rd edition, John Wiley, 1998
-  W. Smythe, *Static and dynamic electricity*, 2nd edition, McGraw Hill, 1950
-  V. Kumar, *Understanding the focusing of charged particle beams in a solenoid magnetic field*, Am. J. Phys. **77** (8) 2009
-  C. Montgomery, R. Dicke, and E. Purcell, *Principles of Microwave Circuits*, McGraw-Hill, 1948
-  N. Mott and H. Massey, *The Theory of Atomic Collisions*, 3rd Edition, p. 229, 1965
-  Ya. S. Derbenev, *RF-resonance beam polarimeter, Part I. Fundamental concepts*, Nuclear Instruments and Methods in Physics Research A 336, 12-15, 1993
-  M. Conte, et al., *The Stern-Gerlach interaction between a traveling particle and a time varying magnetic field*, arXiv:physics/0003069v1 [physics.acc-ph], 2000

-  P. Cameron, et al., *An RF Resonance Polarimeter Phase I Proof of Principle Experiment*, RHIC/AP/126
-  C. Tschalaer, *The Relativistic Stern-Gerlach Force*, arXiv/papers/0802/0802:0154.pdf, 2008
-  C. Tschalaer, *Lorentz Transform of an Arbitrary Force Field on a Particle in its Rest Frame using the Hamilton-Lagrangian Formalism*, BIR#15-01, Bates Lab Report, 2015
-  R. Li and P. Musumeci, *Single-Shot MeV Transmission Electron Microscopy with Picosecond Temporal Resolution*, Physical Review Applied 2, 024003, 2014.
-  D. Cesar et al., *Demonstration of Single-Shot Picosecond Time-Resolved MeV Electron Imaging Using a Compact Permanent Magnet Quadrupole Based Lens*, Phys. Rev. Lett. **17**, 024801, 2016
-  Private communication from P. Musumeci.
-  K. Steffen, *High Energy Beam OPTics*, Interscience, 1966